

because their overall performance can be good. The available literature indicates that the actuated strains of silicone are greater than for any known high-speed electrically actuated material (that is, a bandwidth above 100 Hz). Silicone elastomers also have other desirable material properties such as good actuation pressures and high theoretical efficiencies (80 to 90%) because of the elastomers' low viscoelastic losses and low electrical leakage (12).

The VHB 4910 acrylic adhesive appears to be a highly energetic material. The energy density of the acrylic adhesive is three times that reported for single-crystal lead-zinc niobate/lead titanate (PZN-PT) piezoelectric (about 1 MJ/m³) (1), itself an energetic new material with performance much greater than that of conventional piezoelectrics. The density of both the silicones and the acrylic adhesive is approximately that of water and about one-seventh that of ceramic piezoelectric materials. Hence, the energy density of the acrylic adhesive on a per-weight basis (the specific energy density) is about 21 times that of single-crystal piezoelectrics and more than two orders of magnitude greater than that of most commercial actuator materials.

Potential applications for dielectric elastomer actuators include robotics, artificial muscle, loudspeakers, solid-state linear actuators, and any application for which high-performance actuation is needed. A variety of actuator devices have been made with the silicone elastomers, including rolled actuators, tube actuators, unimorphs, bimorphs, and diaphragm actuators (12, 18, 19). Their performance is promising, but most of this work did not exploit the benefits of high prestrain or the new acrylic material. We have built an actuator using 2.6 g of stretched acrylic film that demonstrated a force of 29 N and displacement of 0.035 m, a high mechanical output for such a small film mass. The very high strains recently achieved suggest novel applications for shape-changing devices, and the specific energy density of the acrylic adhesive is so high that, if it could be realized in a practical device, it could replace hydraulic systems at a fraction of their weight and complexity. However, practical applications require that a number of other issues be addressed, such as high-voltage, high-efficiency driver circuits, fault-tolerant electrodes, long-term reliability, environmental tolerances, and optimal actuator designs.

References and Notes

1. S. Park and T. Shrout, *J. Appl. Phys.* **82**, 1804 (1997).
2. R. H. Baughman et al., *Science* **284**, 1340 (1999).
3. Q. M. Zhang, V. Bharti, X. Zhao, *Science* **280**, 2101 (1998).
4. M. Zhenyi et al., *J. Polym. Sci. B Polym. Phys.* **32**, 2721 (1994).
5. T. Furukawa and N. Seo, *Jpn. J. Appl. Phys.* **29**, 675 (1990).

6. E. Smela, O. Inganäs, I. Lundström, *Science* **268**, 1735 (1995).
7. E. Smela and N. Gadegaard, *Adv. Mater.* **11**, 593 (1999).
8. T. Otero et al., *Proc. SPIE* **3669**, 98 (1999).
9. H. B. Schreyer et al., *Proc. SPIE* **3669**, 192 (1999).
10. K. Oguro et al., *J. Micromachine Soc.* **5**, 27 (1992).
11. H. Tamagawa et al., *Proc. SPIE* **3669**, 254 (1999).
12. R. Kornbluh et al., *Proc. SPIE* **3669**, 149 (1999).
13. R. Pelrine et al., *Sensors Actuators A Phys.* **64**, 77 (1998).
14. For a constant-volume material, $(1 + s_x)(1 + s_y)(1 + s_z) = 1$, where s_x and s_y are the length and width strains. As the film is squeezed, the area of compression $A(s_z)$ can be expressed as $A(s_z) = xy = x_0(1 + s_x)y_0(1 + s_y) = (x_0y_0z_0)/[z_0(1 + s_z)]$, where x_0, y_0 , and z_0 are the initial length, width, and thickness of the active area of the film. The energy density converted to mechanical work is then the integral, over the displacement, of the compressive stress times the area of compression divided by the volume:

$$e = -(1/x_0y_0z_0) \int p A(s_z) dz$$

$$= - \int p [1/(1 + s_z)] ds_z = -p \ln(1 + s_z)$$

where p is the assumed constant compressive stress. The minus sign is introduced because we are defining p as a positive number for compression (dz is negative over the integration). The assumption of constant p depends on the electronic driving circuitry, which ideally would adjust the applied voltage according to the varying thickness to hold the electric field constant. It can be shown that with a nonideal, constant-voltage drive, the term $\ln(1 + s_z)$ would be replaced by $-(s_z + 0.5s_z^2)$. However, because the present focus is on the fundamental material perfor-

mance rather than electronic performance, we make the simplest physical assumption that p is constant.

15. The silicone films are based on a polydimethyl siloxane backbone. They were diluted in naphtha solvent, spin-coated, cured, and released. The HS3 silicone was centrifuged to remove pigment particles before spin coating. VHB 4910 is available in film form with a removable liner backing. The acrylic elastomer is made of mixtures of aliphatic acrylate photocured during film processing. Its elasticity results from the combination of the soft, branched aliphatic groups and the light cross-linking of the acrylic polymer chains. The zero-strain thicknesses of the materials were typically 225 μm for HS3, 50 μm for CF19-2186, and 1000 μm for the VHB 4910 acrylic. The relative dielectric constant at 1 kHz is 2.8 for the two silicones and was measured at 4.8 ± 0.5 for the VHB 4910 acrylic.
16. R. Heydt et al., *J. Sound Vibr.* **215**, 297 (1998).
17. R. Heydt et al., *J. Acoust. Soc. Am.*, in press.
18. R. Kornbluh et al., *Proceedings of the Third IASTED International Conference on Robotics and Manufacturing*, Cancun, Mexico, 14 to 16 June 1995 (ACTA Press, Calgary, Alberta, 1995), pp. 1-6.
19. R. Kornbluh et al., *Proceedings of the 1998 IEEE International Conference on Robotics and Automation*, Leuven, Belgium, May 1998 (IEEE Press, Piscataway, NJ, 1998), pp. 2147-2154.
20. Much of this work was performed under the management of the Micromachine Center at the Industrial Science and Technology Frontier Program, Research and Development of Micromachine Technology of MITI (Japan), supported by the New Energy and Industrial Technology Development Organization.

7 September 1999; accepted 6 December 1999

Two-Dimensional Electronic Excitations in Self-Assembled Conjugated Polymer Nanocrystals

R. Österbacka,* C. P. An, X. M. Jiang, Z. V. Vardeny†

Several spectroscopic methods were applied to study the characteristic properties of the electronic excitations in thin films of regioregular and regiorandom polythiophene polymers. In the regioregular polymers, which form two-dimensional lamellar structures, increased interchain coupling strongly influences the traditional one-dimensional electronic properties of the polymer chains. The photogenerated charge excitations (polarons) show two-dimensional delocalization that results in a relatively small polaronic energy, multiple absorption bands in the gap where the lowest energy band becomes dominant, and associated infrared active vibrations with reverse absorption bands caused by electron-vibration interferences. The relatively weak absorption bands of the delocalized polaron in the visible and near-infrared spectral ranges may help to achieve laser action in nanocrystalline polymer devices using current injection.

Self-assembled organic semiconductor polymers with supramolecular two-dimensional (2D) structures are of interest (1-11) because

the traditional one-dimensional (1D) electronic properties of the π -conjugated polymer chains can be modified by the increased interchain coupling. The regioregular (RR)-substituted polythiophene polymers (7) such as poly(3-alkylthiophene) (P3AT), in which the alkyl side groups are attached to the third position of the thiophene rings in a head-to-tail stereoregular order (Fig. 1A), form thin films with nanocrystalline lamellae (6), resulting in relatively high hole mobilities of $0.1 \text{ cm}^2 \text{ V}^{-1} \text{ s}^{-1}$ (8-11).

Physics Department, University of Utah, Salt Lake City, UT 84112, USA.

*On leave from the Department of Physics and the Graduate School of Materials Research, Åbo Akademi University, Porthansgatan 3, FIN-20500 Turku, Finland.

†To whom correspondence should be addressed. E-mail: val@physics.utah.edu

Thin-film transistors of RR P3AT have already been used to fabricate integrated circuits (8), which, in conjunction with highly luminescent polymers, may also lead to all-organic light-emitting diodes and smart pixels (9). On the contrary, P3AT films of regiorandom (RRa) stereo order (Fig. 1B) do not show supramolecular structures, and the hole mobility is very small, on the order of $10^{-5} \text{ cm}^2 \text{ V}^{-1} \text{ s}^{-1}$ (8–11).

In this work, we applied linear and nonlinear optical spectroscopies to show that the charge carriers (or polarons) in the RR P3AT lamellae become delocalized over several polymer chains, consistent with the high hole mobility. These spectroscopies include photoinduced absorption (PIA), PIA detected magnetic resonance (PIA DMR), doping-induced absorption (DIA), and electroabsorption (EA). In all of these techniques, the changes ΔT in the films' optical transmission T that are induced by the external perturbation were measured versus the photon frequency ω , using phase-sensitive methods, and the absorption modulation spectra $\Delta T(\omega)/T(\omega)$ were obtained. In our measurements, we used visible and near-infrared (NIR) as well as Fourier transform infrared spectrometers. In PIA (12), ΔT is photoinduced by a continuous-wave Ar^+ laser, which generates long-lived photoexcitations with density N . In PIA DMR (12), we modulated the density N by microwave absorption in a magnetic field to obtain the spin state of the photoexcitations that are associated with specific bands in the PIA

spectrum. In the DIA measurements (13), the films were doped by exposure to I_2 vapor for a few seconds. The electric field in EA spectroscopy was on the order of 10^5 V cm^{-1} , and we found a quadratic field-dependent EA in all cases (14).

We studied thin films of RR and RRa P3AT (Fig. 1, A and B), where the alkyl side group $(\text{CH}_2)_n\text{CH}_3$ varied from $n = 4$ to 12. We purchased the P3AT powders from Aldrich, and the films were evaporated from xylene solutions. The RR polymers (>99% head to tail) self-organized to form lamellae perpendicular to the substrate (11), with grain size of $\sim 150 \text{ \AA}$ (6) and high hole mobility (11). The interplane distance b (Fig. 1C) was measured by x-ray diffraction to be $\sim 3.8 \text{ \AA}$, whereas the in-plane, interchain distance a (Fig. 1C) varied from 13 to 27 \AA for $n = 4$ to 12, respectively (6).

In a strictly 1D chain model (15), a single-charge carrier added onto the polymer chain forms a spin $-1/2$ polaron (Fig. 1D), with two localized states in the gap between the lowest unoccupied molecular orbital (LUMO) and the highest occupied molecular orbital (HOMO) (Fig. 1E). The two localized states are shifted inside the gap caused by the polaronic relaxation of the local electronic, bond dimerization (Δr in Fig. 1D), and lattice structure, and thus, polarons have two allowed optical transitions, P_1 and P_2 , (Fig. 1E) below the HOMO-LUMO gap (15). Because of the relatively strong electron-phonon coupling in π -conjugated polymers, the polaron excitation renormalizes the

frequencies of the Raman-active amplitude modes (16), which consequently borrow IR intensity from the electronic transitions. The small polaronic mass causes these IR-active vibrations (IRAVs) to have very large oscillator strengths that are comparable to that of the electronic transitions (17). As seen in Fig. 2A, two DIA bands, P_1 at 0.45 eV and P_2 at 1.3 eV, and associated IRAVs are indeed generated in RR poly(3-hexylthiophene) (P3HT) films upon I_2 doping. The large interstitial iodine ions may actually isolate the polymer chains and cause quasi-1D electronic properties. In addition, the dopant counterion may further localize the induced polaron excitation.

Similar results were obtained upon photo-generation of isolated RR P3HT chains in a polystyrene matrix (Fig. 2B). We observed two correlated PIA bands, P_1 at 0.4 eV and P_2 at 1.35 eV, with associated IRAVs. PIA DMR studies show a spin $-1/2$ resonance with Landé g factor of 2.012 associated with these PIA bands. We therefore conclude that, similar to I_2 doping, the long-lived photoexcitations in isolated RR P3HT chains are localized polarons, with polaronic relaxation energy given by $P_1 \approx 0.35 \text{ eV}$, and 1D electronic properties.

The photoinduced charged excitations in RRa P3HT films are also 1D polarons with P_1

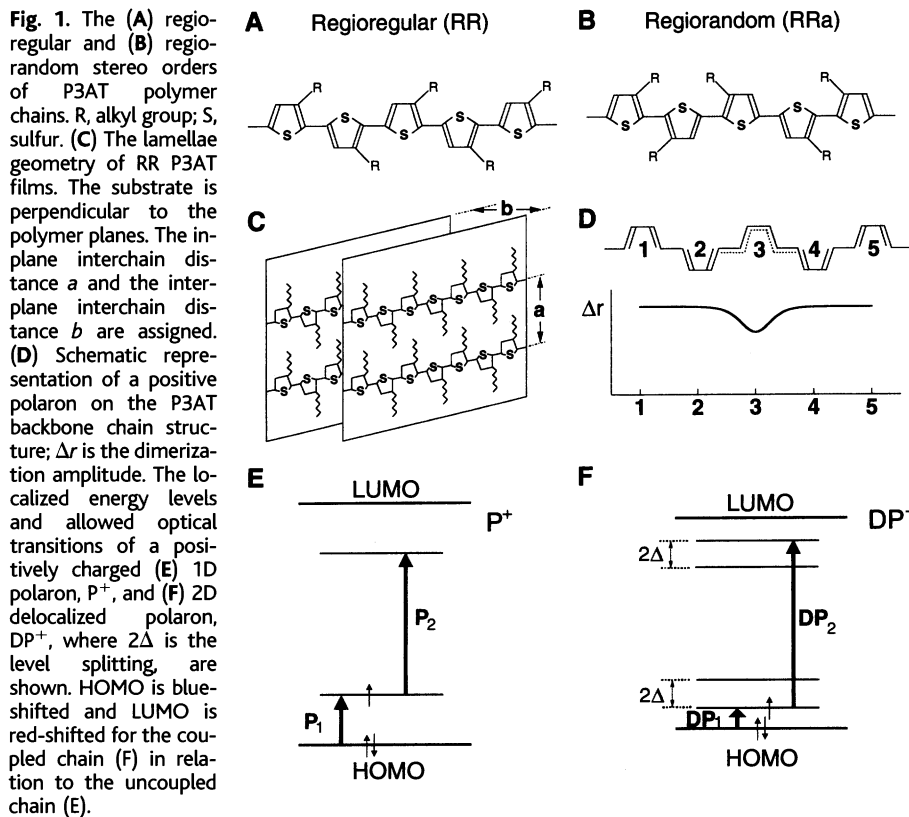


Fig. 1. The (A) regioregular and (B) regiorandom stereo orders of P3AT polymer chains. R, alkyl group; S, sulfur. (C) The lamellae geometry of RR P3AT films. The substrate is perpendicular to the polymer planes. The in-plane interchain distance a and the interplane interchain distance b are assigned. (D) Schematic representation of a positive polaron on the P3AT backbone chain structure; Δr is the dimerization amplitude. The localized energy levels and allowed optical transitions of a positively charged (E) 1D polaron, P^+ , and (F) 2D delocalized polaron, DP^+ , where 2Δ is the level splitting, are shown. HOMO is blue-shifted and LUMO is red-shifted for the coupled chain (F) in relation to the uncoupled chain (E).

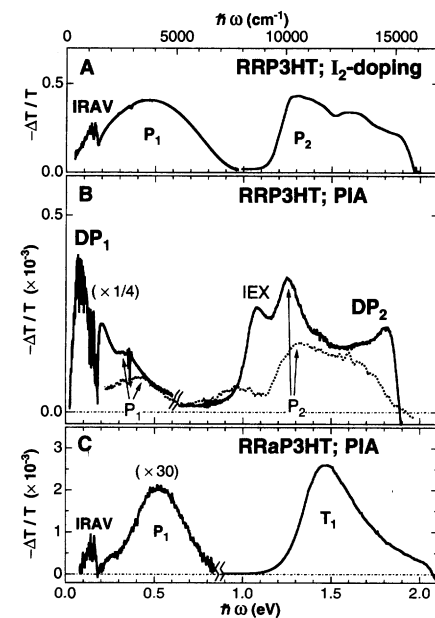


Fig. 2. (A) The DIA bands of RR P3HT film doped with I_2 . Long-lived photoexcitations in films of (B) RR P3HT, where the broken line is for isolated chains in polystyrene, and (C) RRa P3HT, measured by PIA at 80 K, are shown. There is a change in scale at 0.6 eV (B) and 0.85 eV (C). The PIA bands (P_1 and P_2 and DP_1 and DP_2) are associated with 1D polarons (Fig. 1E) and 2D delocalized polarons (Fig. 1F), respectively. IEX and T_1 are related to interchain singlet exciton and intrachain triplet exciton, respectively, whereas IRAVs are IR-active vibrations associated with the 1D polarons. \hbar , Planck's constant divided by 2π .

≈ 0.5 eV and strong IRAVs (Fig. 2C). However, these films also show an improved fluorescence efficiency with a singlet-exciton lifetime on the order of 0.5 ns, which allows efficient intersystem crossing. Thus, the dominant long-lived photoexcitations are triplet excitons with a PIA band at 1.5 eV (Fig. 2C); this excitation was identified in the PIA DMR spectrum by the associated triplet powder pattern at $g \approx 4$ (12). We therefore conclude that the interchain coupling in RRa P3AT films is also weak and results in 1D electronic properties.

However, the PIA spectrum of an undoped RR P3HT film (Fig. 2B), where lamellae are formed (11), substantially differs from those of the other films discussed above. The PIA spectrum shows multiple PIA bands: In addition to the P_1 band at 0.37 eV and the P_2 band at 1.3 eV as in isolated chains in polystyrene, the PIA spectrum in the RR P3HT film also contains three additional PIA bands, denoted DP_1 (for delocalized polarons) with a peak at 0.06 eV (Fig. 2B), interchain excitons (IEXs) at 1.05 eV, and DP_2 at 1.7 eV. The DP_1 and DP_2 PIA bands are correlated: They have the same dependencies on the laser excitation intensity I_L , laser modulation frequency, and temperature. Moreover, we found from PIA DMR measurements that the two DP_i bands (DP_1 and DP_2) are also associated with spin $-1/2$ excitations, but with $g \approx 2.008$, compared to $g \approx 2.012$ for the P_i bands, P_1 and P_2 . The IEX band, however, does not show any PIA DMR and therefore is due to spin singlet excitations. In addition, it is not correlated with the DP_i and P_i

bands and is not generated by charge injection (11). We conjecture, therefore, that the IEX band is due to a neutral, spin singlet excitation. Because intrachain excitons are short-lived in π -conjugated polymers with a lifetime on the order of 1 ns, we think that IEX is caused by interchain excitons (18). We note that the P_i bands are not correlated with the DP_i bands; in addition to a different g value and microwave modulation frequency dependence in PIA DMR, the P_i bands saturate more easily than the DP_i bands with I_L . We therefore conclude that the DP_i bands are due to delocalized polarons in the RR P3HT ordered phase (in the lamellae), whereas the P_i bands are due to localized polarons in disordered P3HT chains surrounding the lamellae.

The influence of increasing the interchain coupling t_\perp on the stability, delocalization, and other electronic properties of polaron excitations in π -conjugated polymer chains has been investigated theoretically (19–24). It has been predicted that, for t_\perp on the order of 0.15 eV, the polaron excitation substantially delocalizes over adjacent chains. Similar to the case of π dimers (25, 26), we assumed that neighboring chains are strongly coupled, which results in an energy splitting 2Δ ($\approx 2t_\perp$) for each of the two polaron levels in the gap, whereas the HOMO-LUMO gap shrinks by the same amount (Fig. 1F). For the two allowed transitions, DP_1 and DP_2 , we then find $DP_1 = P_1 - 2\Delta$ and $DP_2 = P_2 + 2\Delta$, and thus, the sum of the transition energies is conserved; that is, $DP_1 + DP_2 = P_1 + P_2$. Moreover, the intensity ratio of the DP_i transitions is very different from that of isolated polarons, with the lowest energy transition (DP_1) becoming dominant (24). The four

new gap states and associated allowed optical transitions related to a DP^+ excitation (Fig. 1F) can be compared with the DP_i bands of the RR P3HT film (Fig. 2B). We identify two PA bands related to the delocalized polaron excitation, $DP_1 \approx 0.06$ eV and $DP_2 \approx 1.8$ eV, where the DP_1 band is the strongest. We also note that $P_1 + P_2 \approx 1.75$ eV, whereas $DP_1 + DP_2 \approx 1.85$ eV, in agreement with the conservation of the transition energies concluded from the above model.

The DP_1 band (Fig. 2B) is superimposed by narrow bands with some resemblance to the IRAV bands in I_2 -doping films (Fig. 2A) or in PIA of RRa films (Fig. 2C). However, a more detailed examination of the DP_1 band (Fig. 3) indicates that this is not true. First, the narrow superimposed features appear to have negative absorption contributions with antiresonances (ARs) rather than peaks (or resonances), as for regular IRAVs (16, 17). Second, there are many more AR bands than IRAV bands. Third, the AR bands diminish at low frequency, on the DP_1 absorption tail. Finally, the AR frequencies are very near the frequencies of the Raman-active modes and the IR-active modes of the RR P3HT film (Fig. 3). It seems, therefore, that the AR bands are due to Fano-type interferences (27) between the discrete vibrational lines (both Raman and IR active) and the DP_1 electronic band. Such AR bands cannot be described as a set of independent Fano interferences, but the complete phonon propagator has to be considered. In this case, AR bands appear in between each adjacent pair of Raman-active modes (27). Our results differ substantially from this theoretical prediction: First, we observe AR bands with Raman-active mode as well as with IR-active modes. Second, the AR frequencies are very close to the Raman and IR frequencies, indicating a reduced electron-phonon coupling. We speculate that both of these findings may be related to the acquired 2D properties of the delocalized polaron excitation caused by the increased interchain coupling.

Increasing the side-chain length n of the polymers may decrease t_\perp (28) because the interplane interchain separation b (Fig. 1C) increases (6). The change in t_\perp may then be reflected in the delocalized polaron properties: The DP_1 peak energy will increase with decreasing t_\perp (24). The DP_1 band in various RR P3AT films blue-shifts from $n > 6$ (Fig. 3), indicating that, indeed, the delocalized polaron excitation becomes more localized when b increases. However, the DP_1 peak increases again for $n = 4$ [RR poly(3-butylthiophene) (P3BT)]. The reason for this increase is not exactly understood at present; however, it may be related to the difficulties that we encountered in dissolving the RR P3BT powder.

We studied the influence of the increased structural order in RR P3HT films on the intrachain excitons by EA spectroscopy. We found that, in addition to spectral features at 2 eV

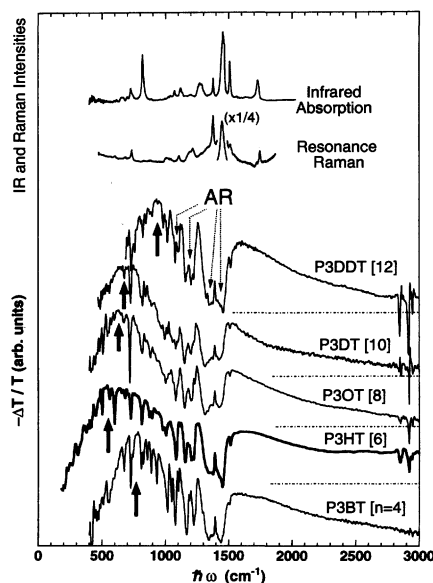


Fig. 3. The DP_1 PIA band in RR P3AT films for alkyl side chains $(CH_2)_nCH_3$ of various length n . Arrows mark the DP_1 peak energy. The resonant Raman scattering and IR absorption spectra of a RR P3HT film are shown for comparison with the AR bands. P3DDT, poly(3-dodecylthiophene); P3DT, poly(3-decylthiophene); and P3OT, poly(3-octylthiophene).

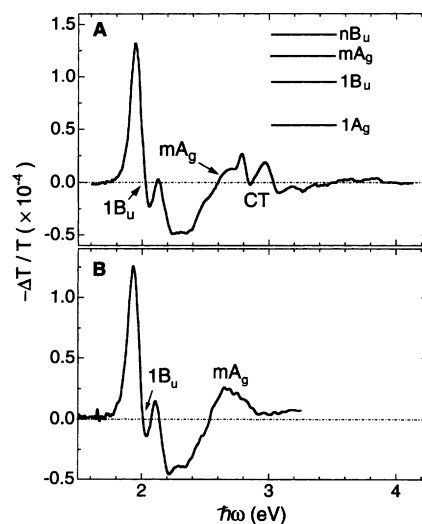


Fig. 4. (A) The EA spectrum of a freshly prepared RR P3HT film. The energies of the intrachain excitons $1B_u$, mA_g , and charge transfer (CT) excitons are assigned. The inset shows the four essential states for explaining the EA spectrum. (B) The EA spectrum of an aged RR P3HT film.

(derivative-like) and 2.7 eV (absorption band), which are similar to those in disordered films (14), the RR P3HT EA spectrum also contains strong oscillation with zero crossing at 2.75 eV (Fig. 4). Such oscillation was previously seen in α -sexithienyl microcrystallites and analyzed in terms of a charge-transfer exciton near the continuum level (29). This may be a prerequisite for the formation of Franz-Keldysh band-edge oscillation, such as in EA of single-crystal polydiacetylene (30). We also found that this oscillation gradually disappears upon aging of the film, due to reduced electron coherence caused by the oxygen attack on the polymer chains (Fig. 4).

In conclusion, we studied and compared long-lived photoexcitations in RR and RRA P3AT films. In RR P3AT films, where lamellae are formed, the increased interplane interchain interaction, t_{\perp} delocalizes the traditional 1D charged polarons onto adjacent chains, acquiring 2D electronic properties. The most prominent optical signature of the delocalized polaron excitation is a strong red-shifted absorption band in the mid-IR range (DP_1) that may be used to directly measure t_{\perp} in polymer films by optical means. In addition, the relatively weak transitions of the delocalized polaron excitation in the visible and NIR spectral range may help to achieve laser action in nanocrystalline polymer devices using current injection, by reducing the optical loss at wavelengths near the exciton-stimulated emission band; so far, this has been an acute problem in the field of plastic lasers. Moreover, although the absorption spectrum of delocalized polaron excitation approaches that of free carriers in more conventional 3D semiconductors, it still contains a low-frequency spectral gap of ~ 60 meV, which is due to the polaronic relaxation and which may be reflected in the relatively low carrier mobility in these films. A further increase of t_{\perp} will close the gap, destabilize the delocalized polaron excitation, and enhance carrier mobility by additional orders of magnitudes. All organic electronic and optoelectronic applications of nanocrystalline π -conjugated polymers may then become a reality.

References and Notes

1. X. Peng, G. Horovitz, D. Fichou, F. Garnier, *Appl. Phys. Lett.* **57**, 2013 (1990); *Adv. Mater.* **2**, 592 (1990).
2. B. Serbet et al., *Adv. Mater.* **5**, 461 (1993); W. Porzio, S. Destri, M. Mascherpa, S. Brucker, *Acta Polym.* **44**, 266 (1993).
3. F. Biscarini et al., *Phys. Rev. B* **52**, 14868 (1995).
4. D. Fichou et al., *Adv. Mater.* **8**, 500 (1996).
5. P. Lane et al., *Chem. Phys.* **210**, 229 (1996); P. Lane et al., *Chem. Phys.* **227**, 57 (1998); G. Lanzani et al., *Phys. Rev. Lett.* **79**, 3066 (1997).
6. T. A. Chen, X. Wu, R. D. Rieke, *J. Am. Chem. Soc.* **117**, 233 (1995); T. J. Prosa, M. J. Winokur, R. D. McCullough, *Macromolecules* **29**, 3654 (1996).
7. R. D. McCullough, *Adv. Mater.* **10**, 93 (1998).
8. Z. Bao, A. Dodabalapur, A. J. Lovinger, *Appl. Phys. Lett.* **69**, 4108 (1996).
9. H. Sirringhaus, N. Tessler, R. H. Friend, *Science* **280**, 1741 (1998); A. Dodabalapur et al., *Appl. Phys. Lett.* **73**, 142 (1998).

10. G. Horovitz, *Adv. Mater.* **10**, 365 (1998).
11. H. Sirringhaus et al., *Nature* **401**, 685 (1999).
12. Z. V. Vardeny and X. Wei, in *Handbook of Conducting Polymers*, T. A. Skotheim, R. L. Elsenbaumer, J. R. Reynolds, Eds. (Dekker, New York, ed. 2, 1997), chap. 22.
13. M. Deussen and H. Bassler, *Synth. Met.* **54**, 49 (1993).
14. M. Liess et al., *Phys. Rev. B* **56**, 15712 (1997).
15. K. Fesser, A. R. Bishop, D. K. Campbell, *Phys. Rev. B* **27**, 4804 (1983).
16. B. Horovitz, *Solid State Commun.* **41**, 729 (1982).
17. E. Ehrenfreund, Z. Vardeny, O. Brafman, B. Horovitz, *Phys. Rev. B* **36**, 1535 (1987).
18. Y. N. Garstein and A. A. Zakhidov, *J. Mol. Electron.* **3**, 163 (1987); H. A. Mizes and E. M. Conwell, *Phys. Rev. B* **50**, 11243 (1994).
19. D. Ermi, *Phys. Rev. B* **33**, 3973 (1986).
20. Yu. N. Garstein and A. A. Zakhidov, *Solid State Commun.* **60**, 105 (1986); *Solid State Commun.* **62**, 213 (1987).
21. D. Baeriswyl and K. Maki, *Synth. Met.* **28**, D507 (1989); *Synth. Met.* **41–43**, 3585 (1991).
22. P. Vogl and D. K. Campbell, *Phys. Rev. Lett.* **62**, 2012 (1989); *Phys. Rev. B* **41**, 12797 (1990).
23. H. A. Mizes and E. M. Conwell, *Phys. Rev. Lett.* **70**, 1505 (1993).

24. J. Blackman and M. K. Sabra, *Phys. Rev. B* **47**, 15437 (1993).
25. Y. N. Gartstein and A. A. Zakhidov, *Synth. Met.* **28**, D501 (1989); *Synth. Met.* **41–43**, 3649 (1991).
26. M. G. Harrison, R. H. Friend, F. Garnier, A. Yassar, *Synth. Met.* **67**, 215 (1994).
27. M. J. Rice, *Phys. Rev. Lett.* **37**, 36 (1976); B. Horovitz, H. Gutfreund, M. Weger, *Phys. Rev. B* **17**, 2796 (1978).
28. The interchain coupling constant t_{\perp} may not be related to the in-plane interchain distance a (Fig. 1C) in a simple way. In fact, it may be a complicated function of n , as was previously realized in the field of charge-transfer salts.
29. L. M. Blinov et al., *Chem. Phys. Lett.* **232**, 401 (1995).
30. L. Sebastian and G. Weiser, *Phys. Rev. Lett.* **46**, 1156 (1981).
31. We thank H. Sirringhaus for sending us a preprint of his work (11) before publication and S. Mazumdar for useful discussions. Supported in part by NSF grant DMR 97-32820 and U.S. Department of Energy grant ER 45490. R.O. acknowledges funding from the Swedish Academy for Engineering Sciences in Finland, the Neste Foundation, and the Ehrnrooth Foundation.

9 September 1999; accepted 9 December 1999

Cool Glacial Temperatures and Changes in Moisture Source Recorded in Oman Groundwaters

Constanze E. Weyhenmeyer,¹ Stephen J. Burns,¹
H. Niklaus Waber,¹ Werner Aeschbach-Hertig,² Rolf Kipfer,²
H. Hugo Loosli,³ Albert Matter¹

Concentrations of atmospheric noble gases (neon, argon, krypton, and xenon) dissolved in groundwaters from northern Oman indicate that the average ground temperature during the Late Pleistocene (15,000 to 24,000 years before present) was $6.5^{\circ} \pm 0.6^{\circ}\text{C}$ lower than that of today. Stable oxygen and hydrogen isotopic groundwater data show that the origin of atmospheric water vapor changed from a primarily southern, Indian Ocean source during the Late Pleistocene to a dominantly northern, Mediterranean source today. The reduced northern water vapor source is consistent with a drier Last Glacial Maximum through much of northern Africa and Arabia.

Large discrepancies exist in estimates of tropical glacial-interglacial temperature changes during the Pleistocene-Holocene transition (1–4). These discrepancies are an obstacle to producing predictive general circulation models (GCMs) of climate. Reconstructions of sea surface temperature (SST) based on transfer function analyses of planktonic foraminiferal assemblages originally indicated that there was less than a 2°C change in tropical SST between the Last Glacial Maximum (LGM) and the Holocene (5–8). Alkenones in deep-sea sediments suggest only a slightly larger glacial-interglacial increase in SST of 2° to 3°C (9, 10). More recent studies of Sr/Ca ratios and $\delta^{18}\text{O}$ (11) records of corals, however, indicate that

tropical SST was as much as 5°C cooler during the LGM than today (12). The coral records are more consistent with available continental paleoclimate studies on vegetation, snow lines, tropical ice cores, and groundwater, which indicate an even larger tropical Pleistocene-Holocene temperature increase of 5° to 8°C (13–20).

SST maps for the LGM are commonly used as boundary conditions for atmospheric circulation models of climate change or as an independent test for GCM simulations (2, 3). Atmospheric circulation models that use CLIMAP SST distributions as boundary conditions generally predict little continental glacial-interglacial temperature changes for tropical regions (2), which is inconsistent with most available geological proxies. More recent simulations with modified SST fields (3) and coupled atmosphere-ocean GCMs (4) that include ocean dynamics (e.g., thermohaline circulation

¹Institute of Geology, University of Bern, CH-3012 Bern, Switzerland. ²Environmental Physics, EAWAG/ETH, CH-8600 Duebendorf, Switzerland. ³Institute of Physics, University of Bern, CH-3012 Bern, Switzerland.